Changes in the Functional and Structural Properties of the Mn Cluster Induced by Replacing the Side Group of the C-Terminus of the D1 Protein of Photosystem II†

Naoki Mizusawa,‡ Toshihiro Yamanari,§ Yukihiro Kimura,‡ Asako Ishii,‡ Shigeaki Nakazawa,‡ and Taka-aki Ono*,‡

Laboratory for Photo-Biology (1), RIKEN Photodynamics Research Center, The Institute of Physical and Chemical Research (RIKEN), 519-1399 Aoba, Aramaki, Aoba, Sendai 980-0845, Japan, and Faculty of Integrated Arts and Sciences, Hiroshima University, 1-7-1 Kagamiyama, Higashi-Hiroshima 739-8521, Japan

Received July 1, 2004; Revised Manuscript Received September 13, 2004

ABSTRACT: A free α-COO^- in the C-terminal alanine-344 (Ala344) in the D1 protein of photosystem II is thought to be responsible for ligating the Mn cluster. The effects of the side group of the C-terminus of the D1 protein on the functional and structural properties of the oxygen-evolving complex (OEC) were comprehensively studied by replacing Ala344 with glycine (Gly), valine (Val), aspartate (Asp), or asparagine (Asn). All the mutants grew photoautotrophically under low-light conditions with lower O_2 evolution activity depending on the mutants when compared with the activity of the control wild type. The Gly-, Asp-, and Asn-substituted mutants did not grow under high-light conditions, while the Val-substituted mutant grew even under the high-light conditions. S_2-state thermoluminescence bands appeared at slightly elevated temperatures when compared with those of the wild type in the Asp- and Gly-substituted mutants, but at almost normal temperatures in the Val- and Asn-substituted mutants. The oxygen-evolving core particles isolated from the mutants showed little change in protein composition. The Gly-, Asp-, and Asn-substituted core particles exhibited low-temperature electron spin resonance (ESR) spectra with reduced S_2 multiline and enhanced $g = 4.1$ ESR signals, while the Val-substituted particles showed a spectrum similar to that of the control particles. Mid-frequency Fourier transform infrared difference spectra showed distinctive changes in several bands arising from the putative carboxylate ligands for the Mn cluster in all substituted particles, but the bands for the putative C-terminal α-carboxylate did not seem to change in the substituted spectra. The changes induced by the Asp and Asn substitution resembled each other except for the amide I region, and showed some similarity to those induced by the Gly substitution in the symmetric carboxylate stretching region. The results were interpreted to mean that similar types of changes of the carboxylate ligands are induced by these substitutions. The band from a putative histidine ligand for the Mn cluster was similarly affected in the Gly-, Asp-, and Asn-substituted spectra, but not in the Val-substituted spectrum. Notably, marked changes in the amide I, amide II, and carboxylate bands were observed in the Val-substituted spectrum, which was different from the Gly-, Asp-, and Asn-substituted spectra. The results indicated that the structural perturbations induced by the Val substitution include large changes of the protein backbone and are considerably different from those induced by the other substitutions. Possible amino acid ligands participating in the changes deduced by Ala344 replacement in the D1 C-terminal and the effects of the changes of the side group on these ligands were considered on the basis of the available X-ray model of the OEC.

Photosynthetic water oxidation takes place in the oxygen-evolving complex (OEC),[1] in which the catalytic center is composed of a tetranuclear Mn cluster located on the lumenal side of the D1 protein. Two water molecules are oxidized to yield an oxygen molecule through five intermediates labeled S_n ($n = 0-4$), where n denotes the number of oxidizing equivalents stored. Each S_n state advances to the S_{n+1} state by absorbing a photon until reaching the highest oxidation state, S_4, which spontaneously reverts to the lowest oxidation state, S_0, concomitant with the release of an oxygen molecule (*1*, *2*). Because the thermally stable S_1 state predominates after prolonged dark incubation, illumination of the dark-adapted OEC with a single flash is accompanied by advancement from the S_1 to the S_2 state. Studies using chemical modifiers (*3*), electron spin−echo envelope modulation (ESEEM) (*4*), and FTIR spectroscopy (*5*, *6*) suggested that histidine and/or acidic amino acids are involved in the ligation of the Mn cluster. Most of the potential ligands to the cluster seem to be located on the D1 protein on the basis of site-directed mutagenesis studies mainly using cyanobac-

† This work was supported by grants for the Frontier Research System and Special Postdoctoral Researchers Programs at RIKEN.

* To whom correspondence should be addressed. Phone: +81 (22) 228 2046. Fax: +81 (22) 228 2045. E-mail: takaaki@postman.riken.go.jp.

‡ RIKEN.

§ Hiroshima University.

[1] Abbreviations: OEC, oxygen-evolving complex; PS, photosystem; Chl, chlorophyll; Q_A, primary quinone acceptor of photosystem II; Q_B, secondary quinone acceptor of photosystem II; FTIR, Fourier transform infrared; ESR, electron spin resonance; DCMU, 3-(3,4-dichlorophenyl)-1,1-dimethylurea; MES, 2-morpholinoethanesulfonic acid; TL, thermoluminescence; PAGE, polyacrylamide gel electrophoresis; SDS, sodium dodecyl sulfate.

10.1021/bi0486076 CCC: $27.50
Published on Web 10/28/2004

terium *Synechocystis* sp. PCC 6803 (reviewed in refs *7* and *8*). These ligands are Asp170, Glu189, His190, His332, Glu333, His337, Asp342, and Ala344 (*9*−*14*), some of which were arranged in close proximity to the Mn cluster in the X-ray structural model of PS II (*15*−*18*).

The D1 protein is synthesized with a short C-terminal extension with the exception of that in *Euglena* and is assembled into the PS II complex (*19*), before being cleaved on the carboxyl side of Ala344 by D1 C-terminal processing protease (CtpA) (*20*). The processing is prerequisite to the light-dependent assembly of the Mn cluster (*21*, *22*), but mutants exhibiting no extension after substituting a stop codon for the amino acid codon at D1-345 (D1-345stop) showed normal photoautotrophic growth and O_2 evolution capability (*10*, *23*). However, none of the C-terminal truncated *Synechocystis* mutants in which Asn335, Asp342, Leu343, and Ala344 were replaced with a stop codon grew photoautotrophically and evolved oxygen (*10*). Therefore, it has been proposed that the presence of the free α-carboxylate in the D1 C-terminal Ala344 is crucial for the assembly of the Mn cluster possibly by ligating one or more Mn ions (*10*). Consistent with this view, the capability of photoautotrophic growth was retained after the site-directed replacement of D1-Ala344 with Gly, Met, Ser, or Val in D1-345stop (=D1-Ala344-stop), although Tyr or Lys substitution led to the loss of the photoautotrophic growth (*10*). The core particles isolated from wild-type *Synechocystis* cells labeled with L-[1-^{13}C]alanine showed that several isotopic bands in the symmetric carboxylate stretching region in the mid-frequency S_2/S_1 FTIR difference spectrum are affected by labeling (*24*). Furthermore, the L-[1-^{13}C]alanine-sensitive bands were absent in particles isolated from the mutants, in which D1-Ala344 was replaced with Gly and Ser, respectively (*24*). The results indicate that the isotope-affected bands can be ascribed to the α-carboxylate group of D1-Ala344, which may be structurally coupled with the Mn cluster as a direct ligand. Ligation of the D1-Ala344 carboxylate to the Mn cluster was also proposed on the basis of the 3.6 Å (*16*) and 3.7 Å (*17*) X-ray structural model. However, the C-terminal carboxylate was arranged in close proximity to a Ca ion in a recent 3.5 Å model, in which a cubane-like Mn_3CaO_4 linked to a fourth Mn by a mono-μ-oxo bridge was proposed, although the C-terminal carboxylate was disordered and not visible on the electron density map (*18*). It may be worthwhile to note in this context that no individual metal ions in the OEC were resolved on any reported X-ray electron density maps, presumably due to some X-ray damage during data collection.

We recently characterized in detail the properties of the OEC in a *Synechocystis* sp. PCC 6803 D1-Ala344Gly-stop mutant in which Ala344 was replaced with Gly (*25*). The mutant grew photoautotrophically under low-light but not under high-light conditions. The Gly substitution led to (i) an upshift of the peak temperatures of the S_2-state thermoluminescence bands, (ii) an enhancement of the S_2 $g = 4.1$ ESR signal with concurrent diminution of the normal S_2 multiline ESR signal, (iii) relatively small but distinctive changes in the bands of the putative carboxylate and histidine ligands for the Mn cluster in the mid-frequency (1800−1000 cm^{-1}) S_2/S_1 FTIR difference spectrum, and (iv) marked changes in the low-frequency (670−350 cm^{-1}) S_2/S_1 FTIR difference spectrum including the Mn−O−Mn mode at 606 cm^{-1}. These results indicate that the internal structure of the Mn cluster and/or the interaction between the Mn cluster and its ligand are considerably altered even with minimal changes in the side group, from methyl (Ala) to hydrogen (Gly) at the C-terminal of the D1 protein (*25*). Replacement of the C-terminal Ala with another amino acid introduces various side groups but may not cause global structural change in the D1 protein. Therefore, these results indicate that the methyl group of D1-Ala344 participates in the manifestation of the proper function and structure of the Mn cluster. The C-terminal replacement can be a potent experimental system for studying functional and structural roles of the methyl group of Ala344 in the OEC by introducing various side groups with limited structural perturbation, and to afford a clue for evaluating whether the carboxylate of the D1 C-terminal Ala344 is a ligand to the Mn cluster.

In the present study, we constructed *Synechocystis* sp. PCC 6803 mutants, in which Ala344 of the D1 protein is replaced with glycine, valine, aspartate, or asparagine (Ala344Gly-stop, Ala344Val-stop, Ala344Asp-stop, Ala344Asn-stop) in a background of a strain lacking the D1 C-terminal extension and having a His tag on the C-terminus of CP47, and then isolated PS II core particles from the mutants. The effects of the substitutions on the properties of the OEC were comprehensively characterized using thermoluminescence, low-temperature ESR, and FTIR. The results were analyzed with regard to how the occupation of various side groups in the C-terminal region influences the functional and structural properties of the Mn cluster.

MATERIALS AND METHODS

Site-Directed Mutants. A host strain for site-directed mutagenesis (B-His/NΔAA) was constructed by replacing part of the *psbA1*, *psbA2*, and *psbA3* genes with DNA fragments conferring resistance to chloramphenicol, spectinomycin, and tetracycline, respectively, and a hexahistidine tag was attached to the C-terminus of the CP47 protein (*25*). Mutations were introduced into the *psbA2* gene of *Synechocystis* sp. PCC 6803 cloned in pNA219, which retains a DNA fragment conferring resistance to kanamycin downstream of the *psbA2* gene as described elsewhere (*25*). Ser345 codon TCT was changed to a stop codon, TGA, for the Ala344-stop strain. For the Ala344Gly-stop, the Ala344Val-stop, the Ala344Asp-stop, and the Ala344Asn-stop strains, Ala344 codon GCG was changed to GGG, GTG, GAC, and AAT, respectively, and simultaneously, Ser345 codon TCT was changed to a TGA stop codon. Plasmids bearing the mutations were transformed into the host strain of *Synechocystis* sp. PCC 6803, and single colonies were selected for their photoautotrophic growth ability on solid BG-11 medium containing 5 μg/mL kanamycin. *Synechocystis* cells were photoheterotrophically grown in liquid BG-11 medium supplemented with 5 mM glucose at 30 °C under 30−50 μmol of photons m^{-2} s^{-1} in an 8 L Clearboy (Nalgene), with bubbling air, up to 7−8 μg of Chl/mL unless otherwise noted.

PS II Core Particles. PS II core particles were prepared from *Synechocystis* cells as previously described (*26*). Briefly, harvested cells were disrupted using a Bead beater (Bio-Spec Products), the resulting thylakoid membranes were solubilized using *n*-dodecyl β-D-maltoside, and PS II particles were then affinity-purified on a Ni−NTA column (Quiagen).

The purified core particles were washed with medium containing 400 mM sucrose, 20 mM NaCl, 5 mM $CaCl_2$, and 20 mM Mes−NaOH (pH 6.0) (medium A) supplemented with 10% (w/v) PEG6000, and were extensively washed and suspended in medium A. For analysis of protein composition, PS II core particles were solubilized using 1% SDS, and were then subjected to SDS−PAGE on a 16−22% gradient gel containing 7.5 M urea (*27*). A sample corresponding to 0.8 μg of Chl was applied to each lane. Peptide bands were visualized by staining with Coomassie Brilliant Blue R-250. The apparent molecular mass of a resolved protein was estimated by comigration of a molecular weight standard (Bio-Rad).

Spectroscopic Measurements. For FTIR measurements, PS II core particles were washed once with medium containing 40 mM sucrose, 5 mM NaCl, 5 mM $CaCl_2$, and 10 mM Mes−NaOH (pH 6.0) and were suspended in the same medium at 2.5−3.5 mg of Chl/mL. The sample suspension (5−8 μL) mixed with 1 μL of sodium ferricyanide solution (100 mM stock) as an electron acceptor was deposited on a BaF_2 disk (20 mm diameter), partially dried under a stream of N_2 gas at 4 °C, and then hydrated in a humidity-controlled FTIR cell as described elsewhere (*25*). The absorbance of the PS II sample was 0.7−1.0 at 1657 cm^{-1} after the dark adaptation for 1 h at 0 °C. The sample temperature was maintained within ±0.03 °C using a homemade cryostat and temperature controller (Chino, KP1000). FTIR spectra were recorded on a Bruker IFS66v/s spectrophotometer equipped with an MCT detector (EG&G Optoelectronics, D316/6) (*25, 26*). A CdTe band-pass filter (2000−350 cm^{-1}) was placed in front of the sample to block the He−Ne laser beam leakage from the interferometer compartment and to improve the signal-to-noise ratio, and a Ge filter was placed at the back of the sample to protect the detector element from laser-scattering. PS II core particles were illuminated with a flash provided from a frequency-doubled Nd^{3+}:YAG laser (Spectra Physics, INDI-50, 532 nm pulse width, 6−7 ns, flash energy ~10 mJ/cm^2). Single-beam spectra (20 scans) were recorded at 4 cm^{-1} resolution before and after the flash. Flash-induced S_2/S_1 difference spectra were calculated by subtracting the single-beam spectrum before the flash from that after the flash. To improve the signal-to-noise ratio, 112−170 difference spectra were averaged.

For ESR measurements, sample cores suspended in a medium containing 400 mM sucrose, 5 mM $CaCl_2$, 5 mM $MgCl_2$, 50 mM Mes−NaOH (pH 6.0), and 0.05 mM potassium ferricyanide at 4 mg of Chl/mL were transferred to a Spracil quartz ESR sample tube, and were illuminated at 213 K for 3 s with a cold light (Hayashi, LA-150TX) passing through a long-pass filter (≥680 nm). Low-temperature X-band ESR spectra were measured using a Bruker E580 spectrometer equipped with an Oxford-900 cryostat and a temperature controller (Oxford, ITC4).

Other Measurements. S_2-state thermoluminescence glow curves were measured using a homemade apparatus as described elsewhere (*28*). Cells were suspended in medium A at 250 μg of Chl/mL in the presence or absence of 0.1 mM DCMU, and illuminated at 0 °C with a saturating xenon flash. The O_2 evolution activity was measured using a Clark-type oxygen electrode in medium A at 25 °C under saturating light conditions supplemented with exogenous electron acceptors, 1 mM 2,5-dimethyl-1,4-benzoquinone and 2 mM potassium ferricyanide for cells or 4 mM potassium ferricyanide for core particles.

Table 1: Photoautotrophic Growth and PS II Activities in D1 C-terminal Mutants of *Synechocystis* sp. PCC 6803

	photoautotrophic growth		oxygen evolution[a]	
strain	low light[b]	high light[c]	cells	PS II cores
Ala344-stop	+++	++++	395 (100)[d]	2400 (100)
Ala344Gly-stop	++	−	350 (89)	1450 (60)
Ala344Val-stop	++	++	350 (89)	1050 (44)
Ala344Asp-stop	+	−	158 (40)	320 (13)
Ala344Asn-stop	++	−	250 (63)	1050 (44)

[a] μmol of O_2 (mg of Chl)$^{-1}$ h^{-1}. [b] 50 μmol of photons m^{-2} s^{-1}. [c] 200 μmol of photons m^{-2} s^{-1}. [d] The numbers in parentheses represent the relative O_2-evolving activity in percent. Low-light grown cells and PS II core particles from the low-light grown cells were used for assays of oxygen evolution.

RESULTS

Effects of Mutations on Physiological and Biochemical Properties. Throughout this study, the Ala344-stop strain which retains Ala344 at the D1 C-terminal with no C-terminal extension and has a hexahistidine tag at the C-terminal of the CP47, was used as a control. The Ala344-stop strain grew photoautotrophically and evolved oxygen at rates comparable with those of the wild-type strain (*25*). As shown in Table 1, all C-terminal mutants examined in this study grew photoautotrophically under low-light conditions. The rates of growth and O_2 evolution differed considerably among the mutants, with the rates ranking as follows: Ala344-stop control > Ala344Gly-stop = Ala344Val-stop > Ala344Asn-stop > Ala344Asp-stop. However, the Ala344Gly-stop, Ala344Asn-stop, and Ala344Asp-stop strains did not grow under high-light conditions, under which the Ala344Val-stop strain grew photoautotrophically. O_2 evolution activities of the PS II particles isolated from the mutants showed the same trends as whole cells, but the activity of the Ala344Asp-stop particles when compared with that of the cells was relatively smaller than with the other mutants. O_2 evolution activity of the Ala344Gly-stop mutant was the same or higher than that of the Ala344Val-stop mutant, indicating that the capability of the photoautotrophic growth under high-light conditions is not directly related to mutation-affected O_2 evolution capability. The activity of each of the PS II particles was not enhanced by further supplementation of the Ca^{2+} and/or Cl^- in medium A.

Figure 1 shows the SDS−PAGE profiles of the PS II core particles from Ala344-stop (lane a), Ala344Gly-stop (lane b), Ala344Val-stop (lane c), Ala344Asp-stop (lane d), and Ala344Asn-stop (lane e) *Synechocystis* cells. All core particles showed very similar protein composition in terms of the major intrinsic proteins including CP47, CP43, D2, D1, and the α subunit of cytochrome b_{559}, as well as the three extrinsic proteins including 33 kDa protein, cytochrome c_{550}, and 12 kDa protein. The particles also showed very similar profiles in the low-molecular-mass bands (<10 kDa), although these bands were diffuse and could not be individually defined. These results demonstrated that site-directed mutations at the C-terminal Ala344 did not substantially affect the protein composition of the OEC, which suggests that no global structural changes in the OEC were induced by the mutations. A protein band at approximately 15 kDa

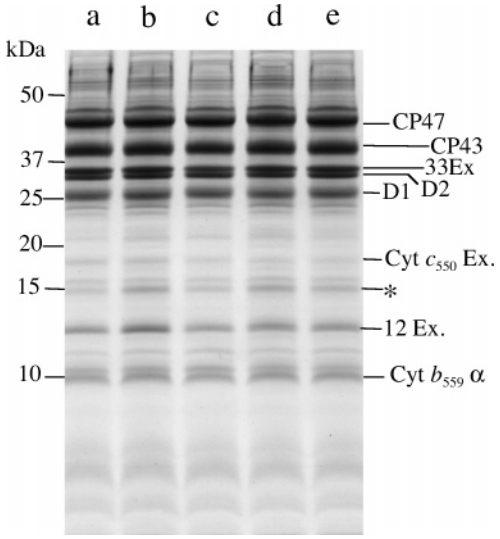

FIGURE 1: SDS−PAGE profiles of PS II core particles from Ala344-stop control cells (a), as well as Ala344Gly-stop (b), Ala344Val-stop (c), Ala344Asp-stop (d), and Ala344Asn-stop (e) mutant cells of *Synechocystis* sp. PCC 6803. A sample containing 0.8 μg of Chl was applied to each lane. Positions of molecular weight standards and PS II proteins are indicated in the left and the right margins, respectively. See the text for a description of the protein band marked with an asterisk.

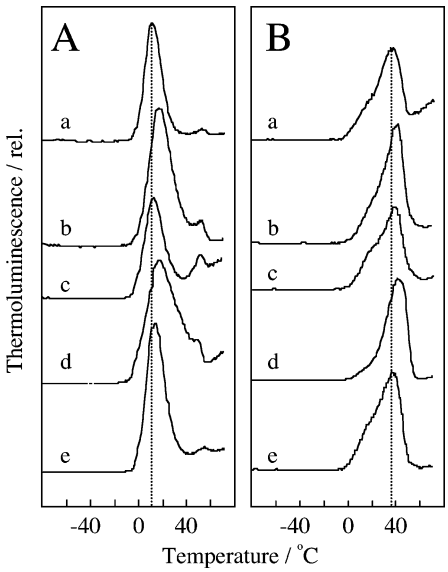

FIGURE 2: Thermoluminescence glow curves for Ala344-stop control cells (a), as well as Ala344Gly-stop (b), Ala344Val-stop (c), Ala344Asp-stop (d), and Ala344Asn-stop (e) mutant cells of *Synechocystis* sp. PCC 6803. Cell suspensions included 0.1 mM (A) or no (B) DCMU for generating an $S_2Q_A^-$ or $S_2Q_B^-$ pair.

(marked by an asterisk in lane e) was an unidentified band sometimes detected at slightly higher amount in the mutant core particles (Figure 1, lanes b and d).

Effects of Mutations on the Functional and Structural Properties of the OEC. The effects of the C-terminal mutations on the redox properties of the Mn cluster were studied by measuring the TL glow curve in the presence (panel A) or absence (panel B) of DCMU as shown in Figure 2. The control Ala344-stop cells (a) showed a 37 °C (−DCMU) and a 10 °C (+DCMU) band due to charge recombination of the $S_2Q_B^-$ and $S_2Q_A^-$ pairs, respectively. Peak temperatures of the S_2 bands in the Ala344Gly-stop (b) and Ala344Asp-stop cells (d) were upshifted by approximately 5 °C for both the $S_2Q_B^-$ and $S_2Q_A^-$ pairs. Notably, the $S_2Q_A^-$ band in the Ala344Asp-stop mutant was relatively broad presumably due to the overlap of another small band with higher peak temperature, although the origin of this band is not clear at present. In contrast, the Ala344Val-stop (c) and Ala344Asn-stop (e) mutants exhibited the $S_2Q_B^-$ and $S_2Q_A^-$ bands with almost the normal peak temperatures. These results indicate that the redox potential of the S_2-state Mn cluster is lowered by replacing the D1 C-terminal Ala344 with Gly or Asp, but not with Val or Asn. The amplitude of the TL bands in the mutants and control cells was not much different despite the relatively large difference in their O_2 evolution activities (Table 1), thus suggesting that lower O_2 evolution activity is not due to lower yields of the S_2 formations in the mutants.

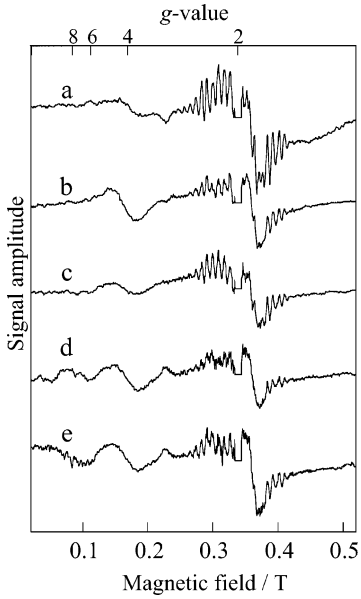

FIGURE 3: Light-minus-dark ESR spectra of the PS II core particles from Ala344-stop control cells (a), as well as Ala344Gly-stop (b), Ala344Val-stop (c), Ala344Asp-stop (d), and Ala344Asn-stop (e) mutant cells of *Synechocystis* sp. PCC 6803. Instrument settings: temperature, 6 K; microwave power, 0.5 mW; microwave frequency, 9.5 GHz; modulation frequency and amplitude, 100 kHz and 1.6 mT, respectively.

Figure 3 shows the light-induced ESR spectra in the control Ala344-stop core particles (a), as well as in the mutant Ala344Gly-stop (b), Ala344Val-stop (c), Ala344Asp-stop (d), and Ala344Asn-stop (e) core particles. The sample particles were illuminated at 213 K, a temperature at which accumulation of the S_2 state is allowed. The Ala344-stop particles showed a prominent $g = 2$ S_2 multiline and a much smaller $g = 4.1$ S_2 signal, as well as an $Fe^{2+}Q_A^-$ signal at $g = 1.9$. A similar spectrum was observed for the Ala344Val-stop particles, although the multiline signal was relatively smaller (∼70%) when compared with that of the control compatible with the lower TL intensity (∼80%) in this mutant cell shown in Figure 2. These observations imply that the amount of active PS II center in this mutant is somewhat lower on a Chl basis (70−80%) as compared with that of the control Ala344-stop. On the other hand, the Ala344Gly-stop, Ala344Asp-stop, and Ala344Asn-stop particles commonly showed spectra with an enhanced $g = 4.1$ and a smaller multiline signal. Notably, no changes in the hyperfine structure of the multiline signal were induced in

any mutant core particles. These results indicate that the Gly, Asp, and Asn substitutions but not the Val substitution induce changes in the magnetic structure of the Mn cluster which facilitate the $g = 4.1$ state. It was reported that the formation of the $g = 4.1$ ESR signal was correlated with the binding of cytochrome c_{550} (*29*). As this protein was preserved in roughly the same amount in every core particle from the mutants as well as the Ala344-stop control as shown in Figure 1, a possible difference in the amounts of this cytochrome among the mutant core particles is not the main cause of changes in intensity of the $g = 4.1$ ESR signal observed in this study.

Figure 4 shows the effects of D1 C-terminal mutations on the mid-frequency S_2/S_1 FTIR difference spectra (panel A, 1800−1200 cm^{-1}; panel B, 1200−1050 cm^{-1}) in the control Ala344-stop core particles (a−d, gray), and the mutant Ala344Gly-stop (a, red), Ala344Val-stop (b, green), Ala344Asp-stop (c, blue), and Ala344Asn-stop (d, magenta) core particles. As shown in panel A, the Ala344-stop spectrum is largely identical to the reported wild-type spectrum (*25*), including changes in the symmetric (1450−1300 cm^{-1}) and asymmetric (1600−1500 cm^{-1}) stretching modes from the putative carboxylate ligands for the Mn cluster as well as the amide I (1700−1600 cm^{-1}) and II (1600−1500 cm^{-1}) modes from protein backbones (*5*, *26*, *30*). The bands from these modes characteristically changed in the respective C-terminal mutants. Ala344Asp-stop (c, blue) and Ala344Asn-stop (d, magenta) mutants showed spectra that were similarly altered when compared with the control Ala344-stop spectrum. In the symmetric carboxylate stretching region, the band at 1363(+) cm^{-1} was largely eliminated, and the 1353(−), 1340(+), and 1327(+) cm^{-1} bands were replaced with a broad featureless positive band. In addition, the intensity of the negative band at 1401 cm^{-1} decreased to some extent. Both mutants also exhibited marked spectral changes in the 1600−1500 cm^{-1} region for the modes of carboxylate asymmetric stretching and amide II. The asymmetric carboxylate band at 1524(−) cm^{-1} was replaced with a positive shoulder at 1520 cm^{-1}, and the 1544-(−) cm^{-1} band was enhanced in both spectra, indicating that the putative carboxylate ligands are similarly affected by these two mutations. In contrast, the effects of mutations on the bands in the amide I region were considerably different between these two mutants; the bands in the Ala344Asp-stop spectrum were largely identical with those in the control Ala344-stop spectrum, but the corresponding bands in the Ala344Asn-stop spectrum were markedly altered.

These features are clearly revealed in panel C, which shows the double difference spectra obtained by subtracting the respective mutant S_2/S_1 FTIR difference spectrum from the control Ala344-stop spectrum (gray). It is obvious that the double difference spectra of Ala344Asp-stop (c) and Ala344Asn-stop (d) were considerably similar to each other. Both the double difference spectra showed a prominent positive band at 1364 cm^{-1} as well as negative bands at 1403 and at 1317 cm^{-1} (Ala344Asp-stop) or 1314 cm^{-1} (Ala344-Asn-stop) in the symmetric carboxylate stretching region. The 1587(+), 1557(−), 1540(+), 1521(−), and 1503(+) cm^{-1} bands in the asymmetric carboxylate stretching and amide II regions in the Ala344Asp-stop double difference spectrum (c) were similarly observed in the Ala344Asn-stop double difference spectrum (d) with slight variations in positions. However, the prominent bands appearing in the amide I region in the Ala344Asn-stop double difference

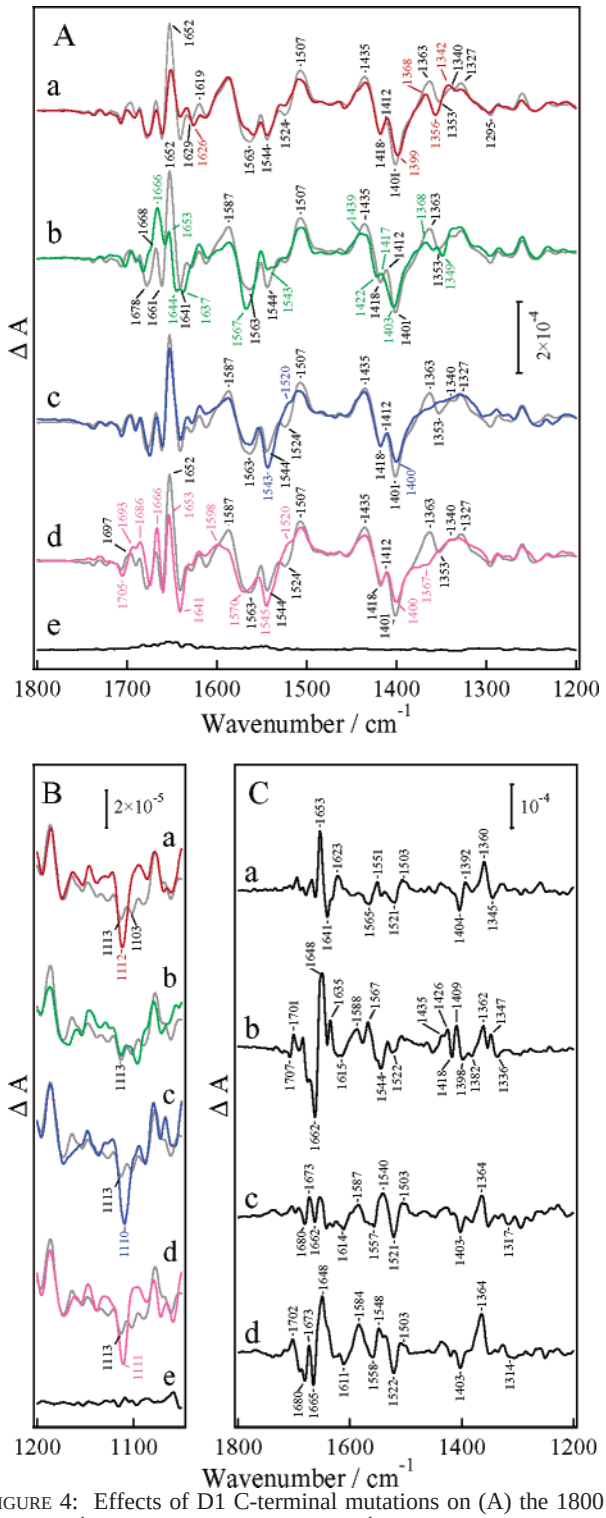

FIGURE 4: Effects of D1 C-terminal mutations on (A) the 1800−1200 cm^{-1} and (B) the 1200−1050 cm^{-1} regions of the S_2/S_1 FTIR difference spectra and (C) the double difference spectra of the PS II core particles. Spectra of the core particles from the Ala344-stop control (gray lines), as well as Ala344Gly-stop (a, red line), Ala344Val-stop (b, green line), Ala344Asp-stop (c, blue line), and Ala344Asn-stop (d, magenta line) mutant cells of *Synechocystis* sp. PCC 6803. Difference spectra were normalized with respect to the peak-to-peak intensity of the 2115(−) cm^{-1} ferricyanide and 2034(+) cm^{-1} ferrocyanide bands. Double difference spectra (panel C, black lines) were obtained by subtracting the respective Ala344-replaced mutant spectra from the Ala344-stop control spectrum. Dark-minus-dark spectra (e) are presented to show the noise levels.

spectrum were not clearly observed in the Ala344Asp-stop double difference spectrum. As shown in panels A and C, the carboxylate stretching and amide bands were also changed in the Ala344Gly-stop spectrum. However, the observed changes in the carboxylate asymmetric stretching and amide II regions were less pronounced than those in the Ala344Asp-stop and Ala344Asn-stop spectra. The double difference spectrum (panel C) showed that the spectral changes in the amide I and II regions induced by the Gly substitution are relatively different from those induced by the Asp and Asn substitution. However, the bands in the symmetric carboxylate region in the Ala344Gly-stop double difference spectrum seemed to show some similarity to those in the Ala344Asp-stop and Ala344Asn-stop double difference spectra; the 1404(−) cm^{-1} band appeared at almost the same position with very similar band intensity, and a distinct positive band appeared at similar frequencies: 1360 cm^{-1} for Ala344Gly-stop, as well as 1364 cm^{-1} for Ala344Asp-stop and Ala344Asn-stop. In contrast to the mutation-affected carboxylate bands, the symmetric carboxylate bands at 1435(+), 1418(−), and 1412(+) cm^{-1} observed in the control Ala344-stop spectrum (panel A, gray) were hardly affected by these mutations, indicating that the mutations do not alter the carboxylate groups responsible for these bands.

As shown in panel A, the Ala344Val-stop spectrum (b, green) was markedly different from the control Ala344-stop spectrum (gray). The 1435(+), 1418(−), 1412(+), and 1363(+) cm^{-1} bands in the symmetric carboxylate region were generally upshifted with some intensity decrease of the 1363(+) cm^{-1} band. Notably, the 1435(+), 1418(−), and 1412(+) cm^{-1} bands were little affected by the Gly, Asp, and Asn substitution. Furthermore, spectral features in the amide and asymmetric carboxylate regions were markedly changed also. Especially, the intense amide I band at 1652(+) cm^{-1} was largely suppressed concomitant with the appearance of the strong 1666(+) cm^{-1} band, and the negative band at 1641 cm^{-1} became a broad band with a double peak at 1644 and 1637 cm^{-1}. As shown in panel C, the Ala344Val-stop double difference spectrum (b) was markedly different from the spectra for the other three mutants, indicating that the changes induced by the Val substitution are considerably different from those induced by the other three substitutions. The double difference spectrum shows the prominent derivative-shaped bands at 1662(−)/1648(+) cm^{-1} in the amide I region, indicating that the Val substitution results in the structural rearrangements of the protein backbone, which induce the upshift of the 1648 cm^{-1} S_2 amide I band to 1662 cm^{-1}, or alternatively the downshift of the 1662 cm^{-1} S_1 amide I band to 1648 cm^{-1}.

Panel B shows the S_2/S_1 FTIR difference spectra at 1200−1050 cm^{-1}, in which the CN stretching mode of the histidine ligand for the Mn cluster appears at 1113 cm^{-1} (*6*, *30*). The histidine band was observed at 1113 cm^{-1} in the control Ala344-stop spectrum accompanied with a much smaller band at 1103 cm^{-1}. This 1103 cm^{-1} band can be ascribed to the side chain modes from the histidine ligands for the acceptor side non-heme iron (*31*, *32*), indicating that a small portion of the non-heme iron oxidized in the dark is reduced by illumination. The Ala344Val-stop spectrum (b, green) was very similar to the control Ala344-stop spectrum (gray), indicating that little structural perturbation is induced in the vicinity of the putative histidine ligand for the Mn cluster by Val substitution. However, the Ala344Gly-stop (a, red), Ala344Asp-stop (c, blue), and Ala344Asn-stop (d, magenta) spectra were considerably similar each other, but commonly altered when compared with the control spectrum, and showed a prominent negative band at 1112−1110 cm^{-1}.

DISCUSSION

The present results clearly demonstrate that the side group of the C-terminal amino acid residue of the D1 protein markedly influences the function and structure of the Mn cluster. The details of the effects of the C-terminal replacement on the structure of the OEC can be evaluated most minutely using vibrational spectroscopy. As shown in Figure 4, the light-induced FTIR difference spectra characteristically changed depending on the amino acid residue on the D1 C-terminal. It has been proposed that symmetric stretching modes of the D1 C-terminal Ala344 α-carboxylate appear at ∼1356 cm^{-1} in the S_1 state and at ∼1339 or ∼1320 cm^{-1} in the S_2 state on the basis of the effects of L-[1-^{13}C]alanine labeling on the S_2/S_1 FTIR difference spectrum (*24*). Furthermore, their band positions indicated that the C-terminal α-carboxylate is a unidentate ligand of the Mn ion which is oxidized during the S_1-to-S_2 transition (*24*). Interestingly, however, these C-terminal modes were not clearly seen in the double difference spectra shown in Figure 4C, in which the mutant spectrum was subtracted from the control spectrum, while the other carboxylate bands appeared more pronouncedly in both the asymmetric and symmetric carboxylate stretching regions. It has been reported that the bands for the symmetric CH_3 deformation and CH bending modes strongly couple to the symmetric carboxylate stretching modes and appear at 1370−1290 cm^{-1} in free alanine in solution (*33*, *34*). They are expected to appear at the same frequency in the double difference spectra, but such a band was not detected. The absence of the putative deformation modes of the Ala344 side group is consistent with little C-terminal α-carboxylate mode in the double difference spectra, even in the Val, Asp, and Asn mutants, in which the side groups are apparently more bulky than the methyl group of Ala344. These results indicate that the C-terminal mutations do not much affect the C-terminal α-carboxylate modes but lead to changes in the other carboxylate groups predominantly. Therefore, it is likely that the methyl group of the C-terminal Ala344 has some role for the proper ligation of the Mn cluster probably independent of the carboxylate group. These observations suggest the close location of the methyl group of Ala344 to the Mn cluster, although the present data do not allow us to determine whether the carboxylate of D1-Ala344 is a ligand to the Mn cluster.

The double difference spectra for the Asp- and Asn-substituted OECs resembled each other as expected from the presence of similar side groups as shown in Figure 4C. They showed very similar bands in the symmetric and asymmetric carboxylate regions, indicating that neither the D1 C-terminal α-carboxylate nor the Mn cluster is structurally coupled with the side group β-carboxylate in the Asp-substituted OEC. However, the spectral changes in the 1702−1611 cm^{-1} region were much more significant in the Ala344Asn-stop than the Ala344Asp-stop spectrum. As these frequencies correspond to the amide I modes, the observed difference may imply that larger perturbation of the protein backbone

is induced in the Asn-substituted than the Asp-substituted OEC. However, this view cannot reconcile with little spectral difference in the amide II region between the double difference spectra for these two mutants (c and d in Figure 4C). Therefore, we think the contribution of the amide I modes to these bands is relatively low. A possible candidate of the origin of the observed spectral changes at 1702−1611 cm^{-1} in the Asn-substituted OEC may be the carbonyl stretching modes of the C-terminal Asn, because carbonyl stretching modes of the Asn side group show relatively strong IR bands at ∼1680 cm^{-1} (*35*, *36*). This implies that the introduction of an extra negative charge in the side group by Asp substitution does not much affect the resulting structural perturbations at least in the S_1 and S_2 states when compared with those by Asn substitution. Therefore, the structural factors of the side groups, including length and volume, are likely to determine mainly the effects of side groups on the Mn cluster at least in the Asp- and Asn-substituted OECs. We note in this context that the functional defects were much more prominent in the Asp-substituted than Asn-substituted OEC as indicated by the lower growth rate and O_2 evolution capability (Table 1) and the upshifted S_2 TL bands (Figure 2) in the Asp-substituted mutant. This may be a consequence of introducing an extra negative charge near the Mn cluster by Asp substitution. Presumably, the presence of the negative charge interferes with the normal S-state cycling beyond the S_2 state.

The double difference spectra revealed that the spectral changes of the symmetric carboxylate region induced by Asp and Asn substitution were somewhat similar to those by Gly substitution. They commonly showed very similar negative bands at 1404 cm^{-1} (for Gly) and 1403 cm^{-1} (for Asp and Asn), and prominent positive bands at relatively similar but not the same frequencies, which were 1360 cm^{-1} for Gly substitution and 1364 cm^{-1} for Asp and Asn substitution. We propose that the symmetric carboxylate region in the Gly-substituted double difference spectrum is explained by the downshift in the control Ala344-stop S_2/S_1 band pair at 1360/1403 cm^{-1} to 1346/1395 cm^{-1} with some decrease in intensity (*25*), as shown in Figure 5Aa and Ba. The main features of the double difference spectra of the Asp- and Asn-substituted OECs are likely to be reproduced to some extent by assuming the downshift of the same 1360/1403 cm^{-1} band pair in the control Ala344-stop to 1317/1367 cm^{-1} for the Asp-substituted spectrum and to 1315/1365 cm^{-1} for the Asn-substituted spectrum as shown in Figure 5Bb and Bc, respectively. However, some difference between the observed and reproduced spectra indicated that other band changes may also overlap in these spectra. According to this scenario, the Gly, Asp, and Asn substitutions seem to affect the structure of the same carboxylate group, which is functional as a ligand of the Mn cluster. D1-Asp342 is a possible candidate affected by the substitutions because the carboxylate group of Asp342 participates in the ligation for the Mn cluster and may be located close to the methyl side group of the C-terminal Ala344 according to the 3.5 Å X-ray structural model (*18*).

Other noticeable changes in the spectral features commonly induced by the Gly, Asp, and Asn substitutions were the appearance of the negative band at ∼1111 cm^{-1} as shown in Figure 4B. In this region, histidine bands from the ligand for the Mn cluster or for the non-heme iron of the acceptor

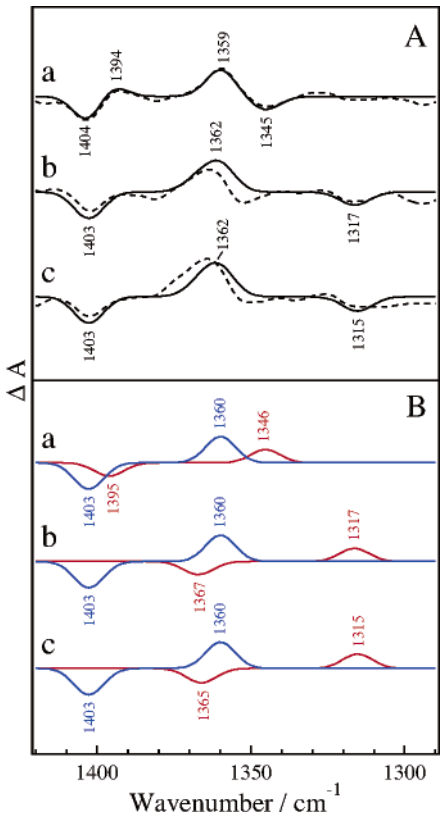

FIGURE 5: Simulation of the double difference FTIR bands for Ala344Gly-stop (a), Ala344Asp-stop (b), and Ala344Asn-stop (c) mutants. (A) Experimentally obtained (dotted lines) and simulated (solid lines) double difference spectra. (B) S_2/S_1 differential band pairs assumed for the Ala344-stop control (blue lines) and mutants (red lines). The same control S_2/S_1 band pair was used for simulation, and double difference spectra were obtained by subtracting the mutant band pair from the control pair. See the text for further details.

side of PS II and bands from buffer molecules appear (*30*). The possibility that this is the buffer band can be excluded because the 1111 cm^{-1} band was not observed in the control Ala344-stop spectrum. Apparently the 1111 cm^{-1} band was distinguishable from the band of the histidine ligands for the non-heme iron appearing at 1103 cm^{-1} (*30*−*32*). This band was partially induced and observed as a small band at 1103 cm^{-1} and was clearly different from the band for the histidine ligand for the Mn cluster at 1113 cm^{-1} in the control Ala344-stop spectrum. The $Y_D^{\bullet}/Y_D$ difference spectrum may show a band at 1103 cm^{-1} (*30*), but the absence of the Y_D tyrosine mode in the double difference spectra indicated the little contribution of this mode in the control Ala344-stop and mutant spectra. Therefore, it is rational to conclude that the 1111 cm^{-1} band is due to the structural coupling of histidine with the Mn cluster. This agrees with the observed isotopic effects on this band (data not shown). Presumably, the histidine ligand for the 1113 cm^{-1} band is affected by mutations to show the intense band at ∼1110 cm^{-1}. A good candidate of the histidine ligand is D1-His332, which has been proposed to ligate the Mn cluster in a position adjacent to D1-Asp342 (*18*). The comparable appearance of the 1111 cm^{-1} band in the double difference spectrum of each mutant indicates that the putative histidine is influenced by the Gly, Asp, and Asn substitutions in the same manner. If we further speculate on the basis of the view that these substitutions similarly affect the carboxylate side group of D1-Asp342,

the ligation by D1-His332 may be influenced by changes in the side group of the D1 C-terminal residue directly and/or indirectly through D1-Asp342. Gly has the minimum side group, while Asp and Asn have linear-like side groups extending more than the side group of Ala. At present, it cannot be decisively described how these so different side groups are arranged and similarly affect the ligands for the Mn cluster, because the resolution of the X-ray model is still not sufficient for dealing with this problem, especially in the D1 C-terminal region (*18*).

The Gly-, Asp-, and Asn-substituted OECs commonly showed increased intensity of the $g = 4.1$ ESR signal and decreased intensity of the multiline ESR signal when compared with the Ala344-stop OEC. This indicates that these substitutions induce similar types of structural changes in the Mn cluster, in which the putative changes in D1-Asp342 and/or D1-His332 may contribute to those of the Mn cluster. It is of note that the Gly substitution induced significant changes in the low-frequency ($670-350$ cm^{-1}) S_2/S_1 FTIR difference spectrum, thus indicating that the internal structure of the Mn cluster and/or the interaction between the Mn cluster and its ligand changed considerably (*25*). Therefore, we believe that the similar changes in the internal structure of the Mn cluster occurred in the Asp- and Asn-substituted OECs, although the direct detection of such structural changes requires low-frequency FTIR measurements, which will be performed in the mutant OEC in the future.

The properties of the Val-substituted OEC were considerably different from those of the other substituted OECs. The Val-substituted mutant grew photoautotrophically even under high-light conditions (Table 1), which is consistent with the normal oxidation potential of the Mn cluster, as revealed by the S_2 TL bands having normal peak temperatures (Figure 2). The S_2 multiline and $g = 4.1$ ESR signals were normally induced, indicating the normal magnetic structure of the Mn cluster (Figure 3). Furthermore, the 1113 cm^{-1} histidine band was induced in the Ala344Val-stop difference spectrum similarly to those in the control Ala344-stop spectrum (Figure 4B). These properties resembled those of the control OEC, and suggest the normal-like Mn cluster in the Val-substituted OEC. In striking contrast, however, relatively large changes were induced in the FTIR bands for the carboxylate, amide I, and amide II modes as shown in Figure 4C. The positions and intensities of the bands in the double difference spectrum for the Val substitution were markedly different from the spectra for the other mutants, indicating that the changes induced in the OEC by the Val substitution are considerably different from those by the other substitutions. The double difference spectrum for the Val-substituted OEC showed prominent bands at $1435-1409$ cm^{-1} in the symmetric carboxylate region, in which few changes were induced for the Gly-, Asp-, and Asn-substituted spectra. Interestingly, these frequencies are similar to those for free carboxylate groups of amino acids (*37*, *38*). Therefore, we presume that the Val substitution leads to changes in the carboxylate groups that are at least partly different from those induced by the other substitutions. The relatively large changes in the amide I and II bands may suggest that some of the changes of the carboxylate groups induced by the mutation are the consequence of the changes of the protein backbone. Taking into account the findings that the structure and function of the Mn cluster were retained relatively normal, the putative protein backbone affected by the Val substitution may position relatively close to the Mn cluster but not be the direct structural constituent of the pocket for the Mn cluster. Presumably, the branched side group of Val sterically hinders the putative protein backbone.

REFERENCES

1. Joliot, P., Barbieri, G., and Chabaud, R. (1969) Un nouveau modele des centres photochimiques du systeme II, *Photochem. Photobiol. 10*, 309−329.
2. Kok, B., Forbush, B., and McGloin, M. P. (1970) Cooperation of charges in photosynthetic O_2 evolution: 1. A linear four-step mechanism, *Photochem. Photobiol. 11*, 457−475.
3. Tamura, N., Noda, K., Wakamatsu, K., Kamachi, H., Inoue, H., and Wada K. (1997) Involvement of carboxyl groups of the PSII reaction center proteins in photoactivation of the apo-water-oxidizing complex, *Plant Cell Physiol. 38*, 578−585.
4. Tang, X.-S., Diner, B. A., Larsen, B. S., Gilchrist, M. L., Lorigan, G. A., and Britt, R. D. (1994) Identification of histidine at the catalytic site of the photosynthetic oxygen-complex, *Proc. Natl. Acad. Sci. U.S.A. 91*, 704−708.
5. Noguchi, T., Ono, T.-A., and Inoue, Y. (1995) Direct detection of a carboxylate bridge between Mn and Ca^{2+} in the photosynthetic oxygen-evolving center by means of Fourier transform infrared spectroscopy, *Biochim. Biophys. Acta 1228*, 189−200.
6. Noguchi, T., Inoue, Y., and Tang, X.-S. (1999) Structure of a histidine-ligand in the photosynthetic oxygen-evolving complex as studied by light-induced Fourier transform difference spectroscopy, *Biochemistry 38*, 10187−10195.
7. Debus, R. J. (2001) Amino acid residues that modulate the properties of tyrosine Y(Z) and the manganese cluster in the water oxidizing complex of photosystem II, *Biochim. Biophys. Acta 1503*, 164−186.
8. Diner, B. A. (2001) Amino acid residues involved in the coordination and assembly of the manganese cluster of photosystem II. Proton-coupled electron transport of the redox-active tyrosines and its relationship to water oxidation, *Biochim. Biophys. Acta 1503*, 147−163.
9. Nixon, P. J., and Diner, B. A. (1992) Aspartate 170 of the photosystem II reaction center polypeptide D1 is involved in the assembly of the oxygen-evolving manganese cluster, *Biochemistry 31*, 942−948.
10. Nixon, P. J., Trost, J. T., and Diner, B. A. (1992) Role of the carboxy terminus of polypeptide D1 in the assembly of a functional water-oxidizing manganese cluster in photosystem II of the cyanobacterium *Synechocystis* sp. PCC 6803: assembly requires a free carboxyl group at C-terminal position 344, *Biochemistry 31*, 10859−10871.
11. Chu, H.-A., Nguyen, A. P., and Debus, R. J. (1994) Site-directed photosystem II mutants with perturbed oxygen-evolving properties. 1. Instability or inefficient assembly of the manganese cluster *in vivo*, *Biochemistry 33*, 6137−6149.
12. Nixon, P. J., and Diner, B. A. (1994) Analysis of water-oxidation mutants constructed in the cyanobacterium *Synechocystis* sp. PCC 6803, *Biochem. Soc. Trans. 22*, 338−343.
13. Chu, H.-A., Nguyen, A. P., and Debus, R. J. (1995) Amino acid residues that influence the binding of manganese or calcium to photosystem II. 1. The lumenal interhelical domains of the D1 polypeptide, *Biochemistry 34*, 5839−5858.
14. Chu, H.-A., Nguyen, A. P., and Debus, R. J. (1995) Amino acid residues that influence the binding of manganese or calcium to photosystem II. 2. The carboxy-terminal domain of the D1 polypeptide, *Biochemistry 34*, 5859−5882.
15. Zouni, A., Witt, H.-T., Kern, J., Fromme, P., Krauss, N., Saenger, W., and Orth, P. (2001) Crystal structure of photosystem II from *Synechococcus elongatus* at 3.8 Å resolution, *Nature 409*, 739−743.
16. Fromme, P., Kern, J., Loll, B., Biesiadka, J., Saenger, W., Witt, H. T., Krauss, N., and Zouni, A. (2002) Functional implications on the mechanism of the function of photosystem II including water oxidation based on the structure of photosystem II, *Philos. Trans. R. Soc. London, Ser. B 357*, 1337−1345.
17. Kamiya, N., and Shen, J.-R. (2003) Crystal structure of oxygen-evolving photosystem II from *Thermosynechococcus vulcanus* at 3.7-Å resolution, *Proc. Natl. Acad. Sci. U.S.A. 100*, 98−103.

18. Ferreira, K. N., Iverson, T. M., Maghlaoui, K., Barber, J., and Iwata, S. (2004) Architecture of the photosynthetic oxygen-evolving center, *Science 303*, 1831−1837.
19. Marder, J. B., Goloubinoff, P., and Edelman, M. (1984) Molecular architecture of the rapidly metabolized 32-kilodalton protein of photosystem II. Indications for COOH-terminal processing of a chloroplast membrane polypeptide, *J. Biol. Chem. 259*, 3900−3908.
20. Shestakov, S. V., Anbudurai, P. R., Stanbekova, G. E., Gadzhiev, A., Lind, L. K., and Pakrasi, H. B. (1994) Molecular cloning and characterization of the ctpA gene encoding a carboxyl-terminal processing protease. Analysis of a spontaneous photosystem II-deficient mutant strain of the cyanobacterium *Synechocystis* sp. PCC 6803, *J. Biol. Chem. 269*, 19354−19359.
21. Taylor, M. A., Packer, J. C. L., and Bowyer, J. R. (1988) Processing of the D1 polypeptide of the photosystem II reaction center and photoactivation of a low fluorescent mutant (LF-1) of *Scenedesmus obliquus*, *FEBS Lett. 237*, 229−233.
22. Diner, B. A., Ries, D. F., Cohen, B. N., and Metz, J. G. (1988) COOH-terminal processing of polypeptide D1 of the photosystem II reaction center of *Scenedesmus obliquus* is necessary for the assembly of the oxygen-evolving complex, *J. Biol. Chem. 263*, 8972−8980.
23. Lers, A., Heifetz, P. B., Boynton, J. E., Gillham, N. W., and Osmond, C. B. (1992) The carboxyl-terminal extension of the D1 protein of photosystem II is not required for optimal photosynthetic performance under CO_2- and light-saturated growth conditions, *J. Biol. Chem. 267*, 17494−17497.
24. Chu, H.-A., Hillier, W., and Debus, R. J. (2004) Evidence that the C-terminus of the D1 polypeptide of photosystem II is ligated to the manganese ion that undergoes oxidation during the S_1 to S_2 transition: an isotope-edited study, *Biochemistry 43*, 3152−3166.
25. Mizusawa, N., Kimura, Y., Ishii, A., Yamanari, T., Nakazawa, S., Teramoto, H., and Ono, T.-A. (2004) Impact of replacement of D1 C-terminal alanine with glycine on structure and function of photosynthetic oxygen evolving complex, *J. Biol. Chem. 279*, 29622−29627.
26. Kimura, Y., Mizusawa, N., Ishii, A., Yamanari, T., and Ono, T.-A. (2003) Changes of low-frequency vibrational modes induced by universal ^{15}N- and ^{13}C-isotope labeling in S_2/S_1 FTIR difference spectrum of oxygen-evolving complex, *Biochemistry 42*, 13170−13177.
27. Ikeuchi, M., and Inoue, Y. (1988) A new 4.8-kDa polypeptide intrinsic to the PSII reaction center, as revealed by modified SDS−PAGE with improved resolution of low-molecular-weight proteins, *Plant Cell Physiol. 29*, 1233−1239.
28. Ono, T.-A, and Inoue, Y. (1986) Effects of removal and reconstitution of the extrinsic 33, 24 and 16 kDa proteins on flash oxygen yield in Photosystem II particles, *Biochim. Biophys. Acta 850*, 380−389.
29. Lakshmi, K. V., Reifler, M. J., Chisholm, D. A., Wang, J. Y., Diner, B. A., and Brudvig, G. W. (2002) Correlation of the cytochrome *c*550 content of cyanobacterial photosystem II with the EPR properties of the oxygen-evolving complex, *Photosynth. Res. 72*, 175−189.
30. Yamanari, T., Kimura, Y., Mizusawa, N., Ishii, A., and Ono, T.-A. (2004) Mid- to low-frequency Fourier transform infrared spectra of S-state cycle for photosynthetic oxygen evolution in *Synechocystis* sp. PCC 6803, *Biochemistry 43*, 7479−7490.
31. Noguchi, T., and Inoue, Y. (1995) Identification of Fourier transform infrared signals from the non-heme iron in photosystem II, *J. Biochem. 118*, 9−12.
32. Hienerwadel, R., and Berthomieu, C. (1995) Bicarbonate binding to the non-heme iron of photosystem II investigated by Fourier transform infrared difference spectroscopy and ^{13}C-labeled bicarbonate, *Biochemistry 34*, 16288−16297.
33. Fukushima, K., Onishi, T., Shimanouchi, T., and Mizushima S. (1959) Assignment of vibration bands of DL-alanine, *Spectrochim. Acta 14*, 236−241.
34. Percy, G. C., and Stenton, H. S. (1976) Infrared band assignments for l-alanine and the nickel (II) and Copper (II) complexes of L- and d-alanine, *J. Chem. Soc., Dalton Trans.* 2429−2433.
35. Venyaminov, S. Y., and Kalnin, N. N. (1990) Quantitative IR spectrophotometry of peptide compounds in water (H_2O) solutions. I. Spectral parameters of amino acid residue absorption bands, *Biopolymers 30*, 1243−1257.
36. Barth, A. (2000) The infrared absorption of amino acid side chains, *Prog. Biophys. Mol. Biol. 74*, 141−173.
37. Deacon, G. B., and Phillips, R. J. (1980) Relationships between the carbon−oxygen stretching frequencies of carboxylate complexes and the type of carboxylate coordination, *Coord. Chem. Rev. 33*, 227−250.
38. Nakamoto, K. (1997) *Infrared and Raman Spectra of Inorganic and Coordination Compounds, Part B: Applications in Coordination, Organometallic, and Bioinorganic Chemistry*, 5th ed., pp 59−62, John Wiley & Sons, New York.

BI0486076